MECHANICAL BEHAVIOR OF SAPPHIRE REINFORCED ALUMINA MATRIX COMPOSITES AT ELEVATED TEMPERATURES

Martha H. Jaskowiak and Jeffrey I. Eldridge
NASA Lewis Research Center
Cleveland, OH

John A. Setlock
Case Western Reserve University
Cleveland, OH

John Z. Gyekenyesi
Cleveland State University
Cleveland, OH

SUMMARY

Zirconia coated sapphire reinforced alumina matrix composites have been tested both after heat treatment to 1400°C and at temperatures ranging from 800°C to 1200°C in air. Interfacial shear stress has also been measured with fiber pushout tests performed in air at room temperature, 800°C and 1000°C. Matrix crack spacing was measured for the tensile tested composites and used to estimate interfacial shear stress up to 1200°C. Electron microscopy was used to determine the source of fiber fracture and to study interfacial failure within the composite.

INTRODUCTION

The primary advantage of an oxide composite is its inherent oxidation resistance. The environmental stability provided by these materials offers the potential for higher operating temperatures without the need for additional oxidation resistant coatings or cooling mechanisms. These capabilities lead to a potential cost and weight savings that make oxide composites particularly attractive to the aerospace industry which requires light weight structural materials with high temperature mechanical and environmental stability.

Limited availability of oxide fiber reinforcement was a determining factor in the choice of composite materials. Oxide fibers are available in either a polycrystalline or single crystal form. The polycrystalline fibers are all smaller in diameter which allows these materials to be woven, infiltrated with a matrix and processed into complex shape parts. These fibers, however, are restricted by microstructural instabilities which result in strength loss and poor creep resistance.

123

The single crystal fibers offer improved microstructural stability and greater strength retention, however, these fibers are only available as larger diameter monofilaments. The large diameter precludes the weaving of the fiber and limits the fabrication of the composite to very simple shapes. Composition of the single crystal fibers which are commercially available in large quantities is presently restricted to alumina. Therefore, in order to utilize single crystal fibers in this study an oxide matrix material with a large coefficient of thermal expansion, such as polycrystalline alumina, was needed.

Incorporation of a single crystal oxide fiber in an oxide matrix of the same composition necessitated the use of a fiber coating to limit fiber to matrix bonding or sintering. Without an interfacial coating acting as a barrier, the sapphire fibers and polycrystalline matrix can sinter. The single crystal fiber grows at the expense of the smaller matrix grains, leaving a roughened interface (ref. 1). Zirconia was selected as a suitable interface based on its thermochemical stability in contact with alumina and its refractoriness. Although phase diagrams exhibit regions of solid solubility between alumina and zirconia at higher temperatures (ref. 2), no evidence of reaction layers or binary compounds formed between the alumina and zirconia were apparent in any of the samples which were processed or fabricated at temperatures up to 1400°C. Pure zirconia was proven to be both chemically stable in contact with sapphire and mechanically capable of providing a weak interfacial layer between fiber and matrix (ref. 1). Further thermal exposure of composite samples established the long term thermal stability of the zirconia fiber coatings. Composite strength reached a threshold level after approximately 48 hours at 1400°C. Grain size of the zirconia also reached a maximum at this point. After the microstructure of the ZrO_2 interface stabilized, composite strengths also approached a relatively contant level (ref. 3).

The next step in the evaluation of these composites was to investigate high temperature mechanical properties. The objective of this work was to measure composite tensile and interfacial properties at temperatures that could affect individual components of the composite. Electron microscopy was used to interpret the results and understand the mechanical behavior at temperature.

EXPERIMENTAL PROCEDURES

C-axis sapphire fibers with a mean diameter of approximately 132 microns (5.2 mils) were purchased from Saphikon, Inc. Unstabilized zirconia coatings were applied to the fibers by MSNW, Inc. The thickness of the sol-gel derived zirconia coatings was approximately 1.5 to 2.0 microns. The adherence of the coating resulted in uniform and continuous coverage along the fiber surface. The matrix was produced from high purity alumina powders which were combined with organic binders and ball milled to produce a slurry of submicron size particles. The slurry was tape cast and cut into 15.25 cm (6.0 in) lengths. Zirconia coated fibers were wound on a drum, coated with the matrix precursor and also cut into 15.24 cm (6.0 in) long mats. The fiber mats and tapes were then stacked in the appropriate proportions and hot pressed to yield a unidirectional fiber reinforced composite with an approximate fiber volume fraction of 30%.

Composites tensile samples, which were flat bars with straight sides, were tabbed at both ends for gripping. Tabs were cut from graphite fiber reinforced PMR-15 and bonded to the tensile samples by a heat activated activated adhesive. The tabbed ends of the specimen were held in water cooled grips outside of the furnace. The samples were 15 cm (6.0 in) long, 1.3 cm (0.5 in) wide and approximately 0.203 cm (0.080 in) thick. The composites were tensile tested in air at room temperature, 800°C and 1200°C. The furnace hot zone is approximately 25 mm (1.0 in) in length. The composites were tested under load control with a loading rate of 1 kN/min.

Interfacial shear stress (ISS) was determined from both fiber push-out tests and from calculations based on matrix crack spacing measured from composite tensile samples. The fiber push-out tests were performed in air at room temperature, 800°C and 1000°C in a high temperature fiber push-out apparatus designed by Eldridge (ref. 4). In this apparatus, the sample and indenter are located within a vacuum chamber. The indenter was a cylindrical tungsten carbide punch with a flat bottom. Diameter of the punch was 100 microns. Sample heating was accomplished by a quartz halogen lamp which was situated outside of the vacuum chamber. An ellipsoidal reflector was used to focus the heating radiation. The hot zone was a spot with a diameter of approximately 1.3 cm (0.5 in). As in the room temperature tests, which have been described previously (ref. 5), the indenter was driven by a constant displacement rate mechanism.

Scanning electron microscopy (SEM) analysis was used to observe microstructural changes and interpret the resulting composite behavior. Composite tensile fracture samples were examined to identify changes in fiber pull out length and measure matrix crack spacing. Primary fiber fracture surfaces were also identified from the composite tensile samples. Location of fiber fracture origins and critical flaw sizes were determined from these samples. Push-out samples were also studied with the SEM. The location of the failure within the interfacial region was determined by studying both the pushed in and pushed out sides of the test samples.

RESULTS AND DISCUSSION

A cross-section of the as-fabricated composite (fig. 1) displays the random distribution of the sapphire fibers. The sol-gel derived ZrO_2 coatings remain intact on the fiber surface after winding and composite fabrication. Throughout the study of these composites it was attempted to keep the fiber volume fractions at a constant level of approximately 30 %. In the current set of composites fabricated for high temperature testing, however, fiber volume fractions were slightly lower than the desired levels. Fiber volume fractions ranged from 25 to 27 %. The thermal stability of the zirconia coated fibers is displayed in fig. 2. Uncoated and zirconia coated sapphire filaments were heat treated under similar conditions and subsequently tensile tested in air at room temperature. Each data point represents approximately 15 to 20 single fiber tests with a 0.64 cm (0.25 in) gauge length. After thermal exposure at 1400°C for 100 hours the coated fibers possess tensile strengths similar to those of the uncoated fibers treated under the same conditions. Therefore, for the temperatures and times studied in this work, the zirconia coatings did not cause any additional degradation of the fiber strength.

The ability of the zirconia coatings to limit interfacial bonding and therefore improve composite toughness and strength is dramatically represented in the stress versus strain curves of fig. 3. Without fiber coatings the composite fails in a brittle manner with no fiber pull out. Average tensile strength for these composites was 130 ± 49 MPa. The utilization of a zirconia fiber coating in this system resulted in a substantial increase in both composite stress and strain. Average tensile strength rose to 421 ± 36 MPa. Modulus for these composites was 158 ± 9 GPa. Although heat treatment of these composites resulted in grain growth of the zirconia fiber coating, the interface maintained its ability to provide crack deflection and fiber pull out. Composite tensile strength was measured at 306 ± 22 MPa after treatment at 1400°C for 200 hrs in air (fig. 4). This value represents a strength retention of approximately 73 % of their as-produced strength.

Tensile strengths and moduli of the composites tested at room temperature, 800°C and 1200°C are displayed in fig. 5. The as-fabricated tensile strength of these composites, 215 ± 70 MPa, was slightly lower than anticipated. This difference in as-fabricated strengths between these composites and those previously measured is due largely to the lower fiber volume fractions of the composites in this study. Although fiber volume fractions of 30 % or higher were desired, the current fiber volume fractions were on the order of 25 to 27 %, while the previously tested samples had fiber volume fractions of 33 to 35 %. The lower fiber volume fractions were the result of subtle differences in matrix processing which resulted in higher yields from the alumina slurry and thicker tapes. In fig. 5, the composite tensile strength decreases from 215 MPa at room temperature to 86 MPa at 1200°C. Since the composite tensile strength is a fiber dominated property, the decrease in composite strength can be directly correlated with fiber behavior at these temperatures (fig. 6). Sapphire fibers suffer strength losses until they reach a level of approximately 689 MPa (100 ksi) at temperatures beyond 1200°C. It is anticipated that at higher test temperatures (from 1200 to 1400°C), the composites would also maintain a baseline strength similar to the behavior of the fibers.

By using the simple rule of mixtures, a room temperature composite modulus can be calculated. Reported modulus values for sapphire vary from 460 GPA, measured parallel to the c-axis (ref. 6), to 400 GPa, for pore free commercially available material (ref. 7). By using an empirically derived value of 59 GPa for the porous alumina matrix and considering the range of reported values for sapphire , the modulus for a composite reinforced with 25.5 % volume fraction of fibers varies from 146 to 161 Gpa. The measured value of 154 ± 8 GPa for a room temperature composite tensile test is in close agreement with this range of estimated values from the rule of mixtures. The decrease in composite modulus at 800°C and 1200°C reflects the general temperature dependence of the modulus of monolithic polycrystalline alumina and sapphire (ref. 8).

Fiber pull out was readily observed in the composites tested at room temperature and 800°C (fig. 7). At 1200°C, fiber pull out was reduced substantially but not eliminated. Fracture surfaces revealed pull out lengths of 1 mm or less. The reduced pull out length is believed to be caused by a combination of higher interfacial shear stress and lower fiber strength. Close examination of the pulled out fibers indicates the tendency of the fiber coating to remain with the fiber. Study of selected areas of the fiber surface where the coating was absent reveal very little pitting of the sapphire fiber (fig. 8). Past studies demonstrated the tendency of the zirconia to cause pitting of the sapphire after prolonged thermal exposures (ref. 9). In specific cases the cause of this surface

126

degradation was attributed to the presence of an impurity induced transient liquid phase capable of altering the surface of the sapphire. However, even in the absence of this liquid phase and with no reaction layer present, surface degradation was still observed. Therefore, it is believed that solid state interactions between the unstabilized zirconia and sapphire may also induce pitting of the fiber surface (refs. 10 and 11). Although this pitting caused little additional fiber strength loss it did result in increased mechanical gripping of the fiber and higher ISS values. In the current study, however, with only short term exposure to the testing temperature, little or no surface damage to the fibers was observed.

Study of primary fiber fracture surfaces from composite tensile tests gave further proof that the fiber surfaces were unharmed by the processing or testing conditions. For roughly 80 % of the fibers examined, matching primary fracture surfaces (both halves of the same fiber) were identified (fig. 9). From all of the fracture surfaces, only internal voids were determined to be the critical flaws causing fiber failure (fig. 10) regardless of test temperature. These voids were created during fiber fabrication. There appeared to be no surface flaws capable of causing fiber failure. The majority of internal flaws were approximately 1 micron voids. Occasionally, flaws up to 10 microns were observed.

Fiber push-out tests performed at room temperature resulted in debonding and sliding of the fibers without matrix or fiber cracking (fig. 11). The load versus displacement curve of fig. 12 displays a linear region up to point (1). At this point, debonding begins. The non-linear region of the curve up to point (2) may indicate crack propagation at the fiber/matrix interface. Finally, a linear region after point (3) indicates frictional sliding of the fiber. At room temperature, similar debonding and frictional shear stresses were measured, both in the 50 to 60 MPa range (fig. 13). The average interfacial shear stress measured at 800°C was 62 ± 7 MPa. By using previously derived equations for the case of multiple matrix cracking (ref. 12), and crack spacings of 332 and 208 microns, interfacial shear stresses were estimated as 40 and 55 MPa for the composites tensile tested at room temperature and 800°C, respectively. Both values support the empirically derived values for these test temperatures.

At 1000°C it became impossible to push the fibers out of the matrix because of plastic deformation mechanisms which become active in sapphire at these temperatures. Micrographs of the pushed in side of the fiber show the imprint of the indenter and evidence of possible twinning in the sapphire (fig. 14a). The other side of the push-out sample showed no evidence of the fiber being dislodged or of debonding in the interfacial region. Essentially the fiber was compressed leaving the other side of the sample completely featureless. Careful examination of the fiber from the pushed in side shows that debonding has occurred within the interface (14b). It is believed the initiation of debonding was detectable on the load versus time curve (fig. 15). Plastic deformation that occurred within the sapphire after this point made it impossible to measure further debonding or frictional shear stresses. Therefore the shear stress assigned to the 1000°C push-out tests, approximately 50 MPa, merely represents the initiation of debonding, not sliding of the entire fiber as was the case for the tests at room temperature and 800°C. By further examination of the 1000°C push-out samples in the SEM, it was observed that the zirconia remains capable of producing crack deflection around the fibers (fig. 16). Even though the push-out tests at 1000°C were not capable of providing quantitative information regarding debonding and frictional shear stresses, useful

information describing the interaction of cracks with the zirconia interface was gained. By measuring matrix crack spacing from composite samples tested in tension at 1200°C, interfacial shear stress was estimated to be approximately 106 MPa. The increase in interfacial shear stress was verified by the decrease in fiber pull out which was observed at these temperatures.

CONCLUSIONS

The composite strength loss at elevated temperatures can be directly related to the fiber behavior at these temperatures. The need for advanced fibers with improved high temperature properties is further emphasized by these results. Although quantitative measurement of interfacial shear stress was not possible beyond 800°C, fiber debonding and crack deflection observed in these samples indicate that zirconia remained effective as an interfacial material for a sapphire reinforced alumina matrix composite.

REFERENCES

1. Jaskowiak, M.H.; Eldridge, J.I.; Philipp, W.P.; and Setlock, J.A; Effectiveness of ZrO_2 Interfacial Coatings for Tough Sapphire/Al_2O_3 Composites, NASA TM 105782, 1992.

2. Alper, A.M., Inter-Relationship of Phase Equilibria, Microstructure and Properties in Fusion-Cast Ceramics. Science of Ceramics, Vol. 3, G.H. Stewart, ed., Academic Press Inc., London, 1967, p. 339.

3. Jaskowiak, M.H.; Setlock, J.A.; Processing and Mechanical Properties of Sapphire Reinforced Alumina Matrix Composites, HiTemp Review 1994; Advanced High Temperature Engine Materials Technology Program, NASA CP-10146, 1994, pp.59-1 to 59-12.

4. Eldridge, J.I., Elevated Temperature fiber Push-Out Testing, Mat. Res. Soc. Symp. Proc. Vol. 365, 1995, pp.283 - 290.

5. Eldridge, J.I.,; Bhatt, R.T.; and Kiser, J.D.; Investigation of Interfacial shear Strength in SiC/Si_3N_4 Composites, NASA TM-103739, 1991.

6. Morrell, R., Handbook of Properties of Technical and Engineering Ceramics, Part 1 An Introduction for the Engineer and Designer, Her Majesty's Stationery Office, London, 1985.

7. Morrell, R., Handbook of Properties of Technical and Engineering Ceramics, Part 2 Data Reviews, Section 1 High-Alumina Ceramics, Her Majesty's Stationery Office, London, 1987.

8. Gitzen, W.H., ed., Alumina as a Ceramic Material, The American Ceramic Society, Special Publication No. 4, 1970.

9. Jaskowiak, M.H., Hyatt, M.J., Philipp, W.H., Eldridge, J.I., Setlock, J.A.; Effects of ZrO_2 Interfacial Coatings in Al_2O_3/Al_2O_3 Composites, HiTemp Review 1990, NASA CP 10051, 1990, pp.60-1 to 60-12.

10. Stough, M.A.; Hellmann, J.R.; Diffusion analysis in the Alumina/Zirconia System, HiTemp Review 1995; Advanced High Temperature Engine Materials Technology Program, NASA CP-10178.

11. Stough, M.A.; Hellmann, J.R.; Solid solubility and diffusion in Zirconia/Sapphire Interfaces, HiTemp Review 1994; Advanced High Temperature Engine Materials Technology Program, NASA CP-10146,1994, pp.60-1 to 60-11.

12. Kimber, A.C.; Keer, J.G.; On the Theoretical Average Crack Spacing In Brittle Matrix Composites Containing continuous aligned Fibers, J. Mat. Sci. Let., Vol. 1, 1982.
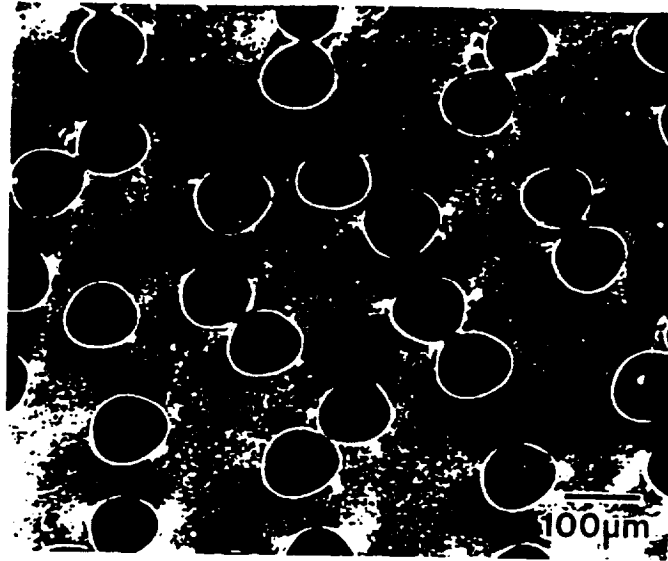
Figure 1. Cross section of as-fabricated composite displaying random distribution of ZrO₂ coated sapphire fibers.
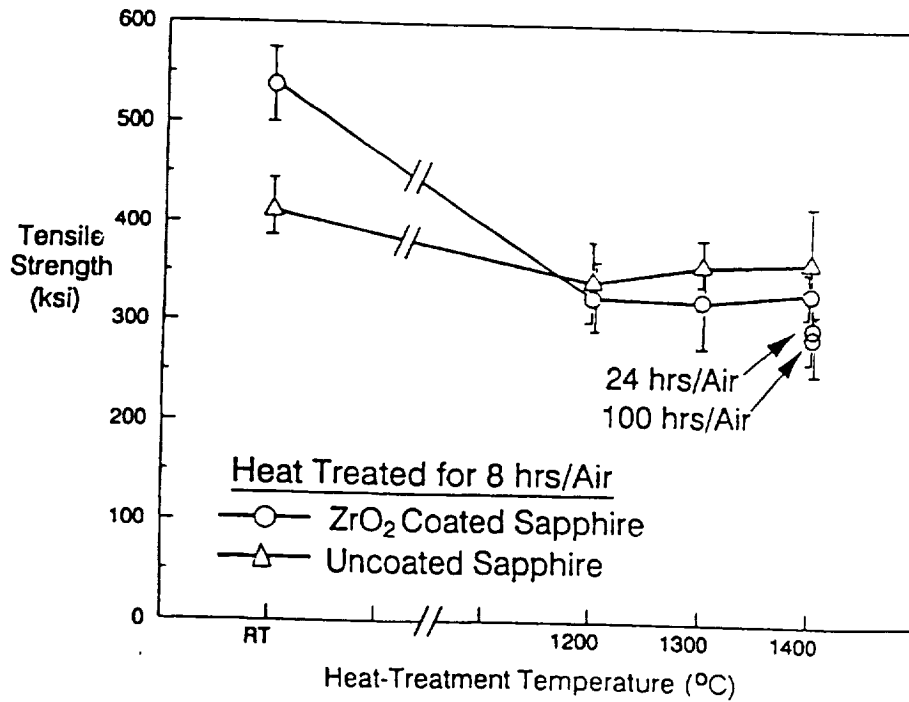
Figure 2. Room temperature residual tensile strengths of ZrO₂ coated and uncoated sapphire fibers after heat treatment in air.
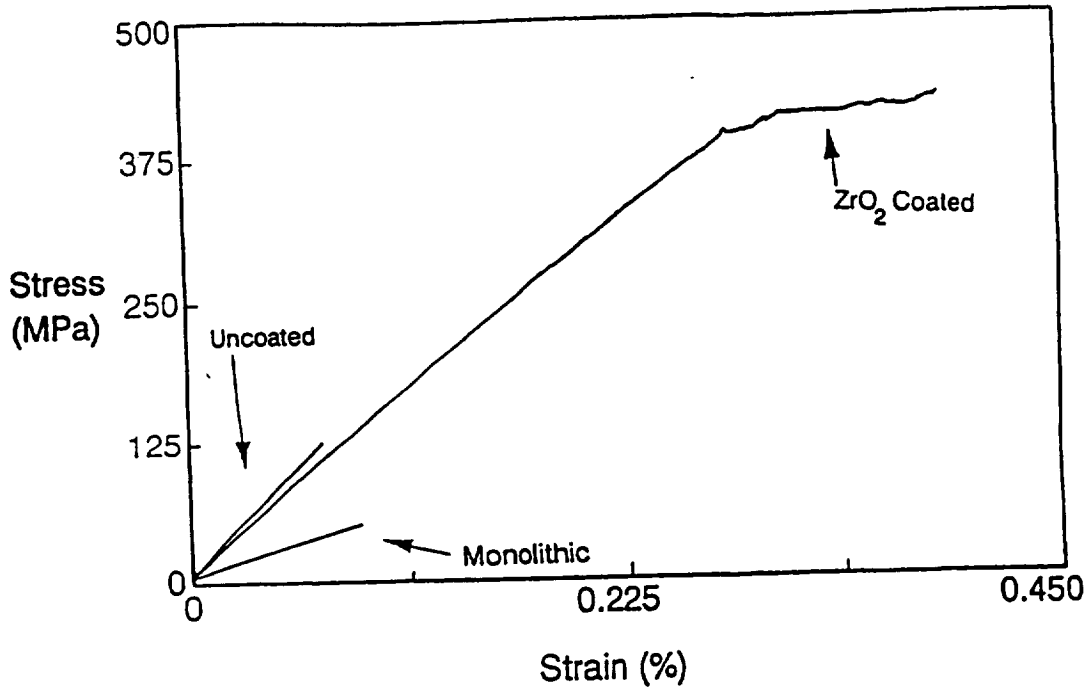
Figure 3. Stress vs. strain curves for room temperature tensile tests of as-fabricated monolithic alumina and alumina matrix composites reinforced with either uncoated or ZrO_2 coated sapphire fibers.
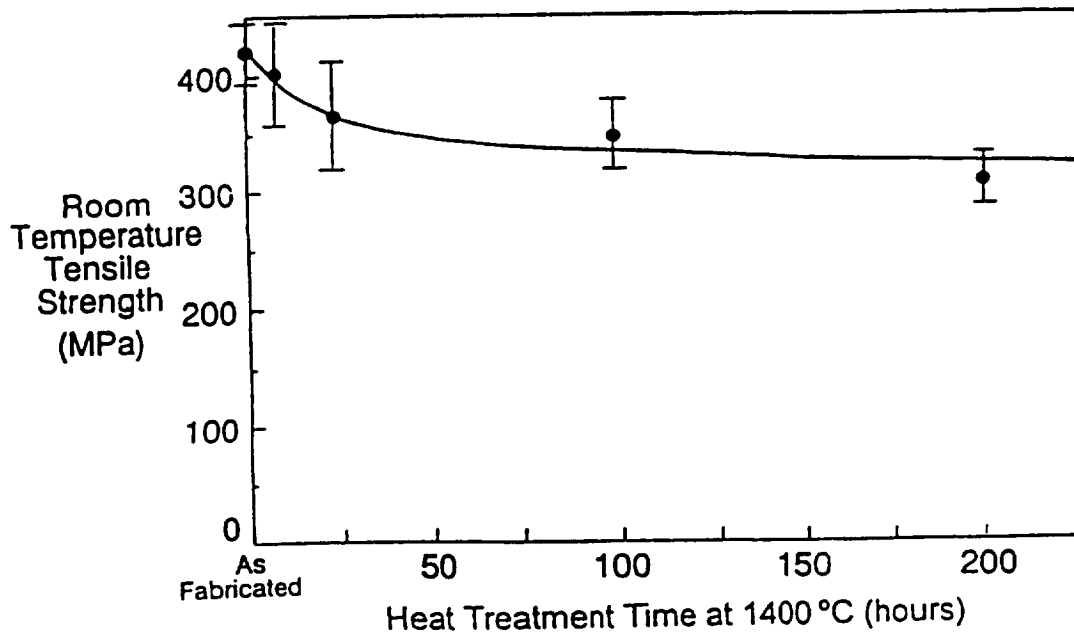

Figure 4. Room temperature residual tensile strengths of ZrO_2 coated sapphire fiber reinforced Al_2O_3 matrix composites after heat treatment in air at 1400°C.

131
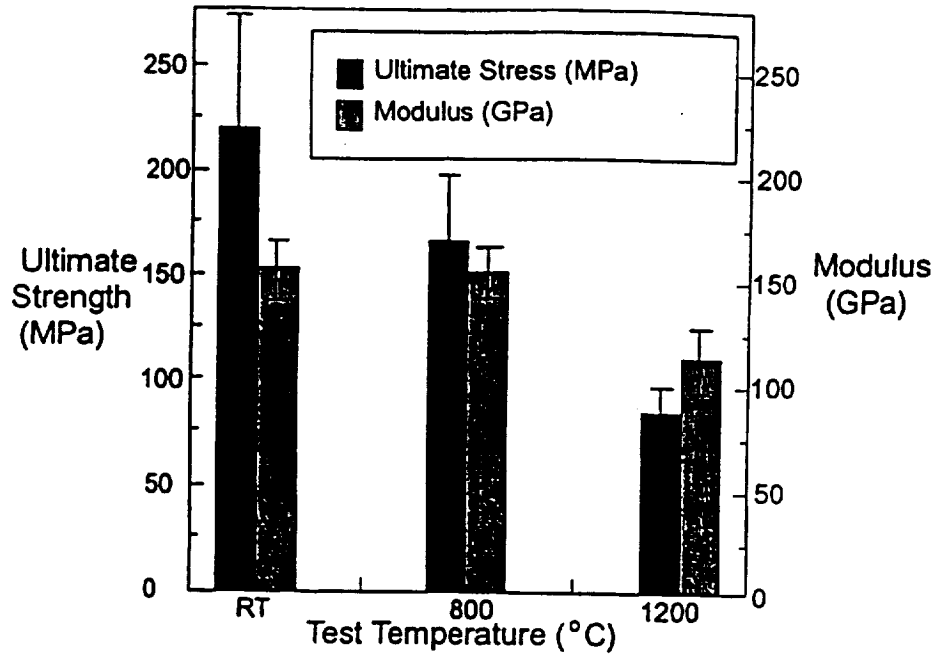
Figure 5. Tensile strengths and moduli of ZrO_2 coated sapphire fiber reinforced alumina matrix composites tested at temperature in air.
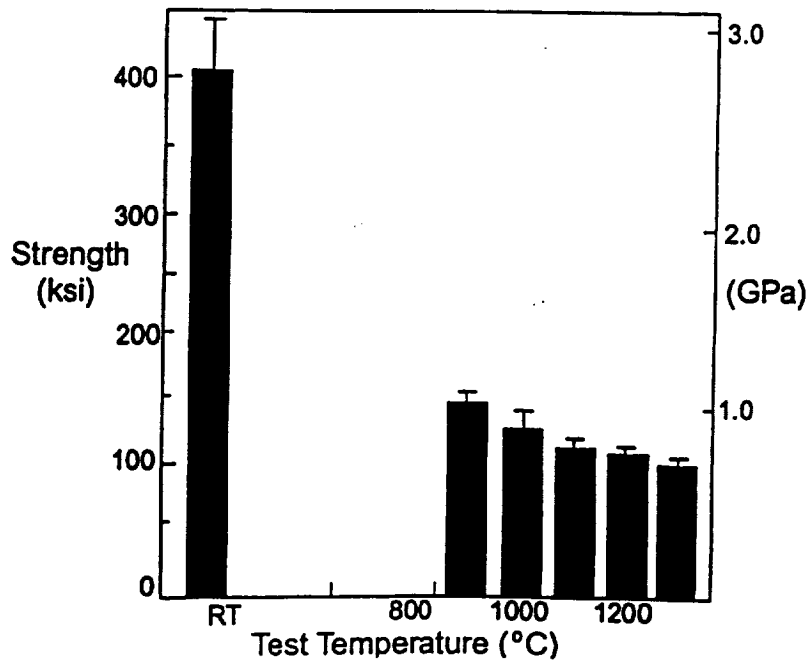
Figure 6. Tensile strengths of sapphire fibers tested at temperature in air.

1200°C Fracture Surface

RT

800°C

1200°C

1 mm
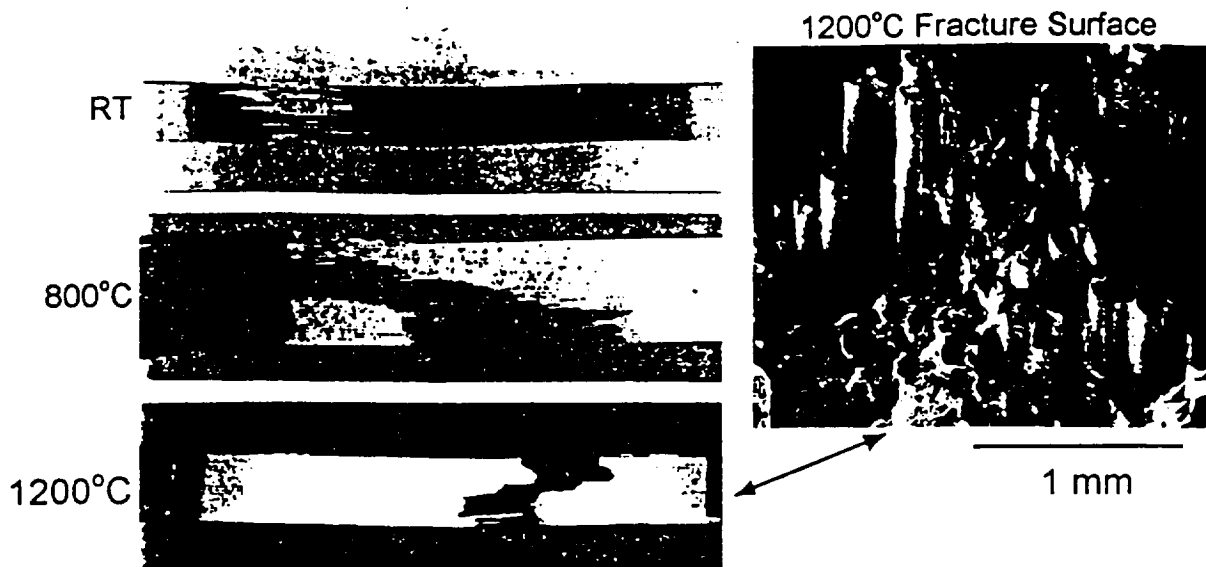
Figure 7. Tensile fracture surfaces from composites tested at room temperature, 800°C, and 1200°C. High magnification view of reduced fiber pull-out length from 1200°C tensile tests.
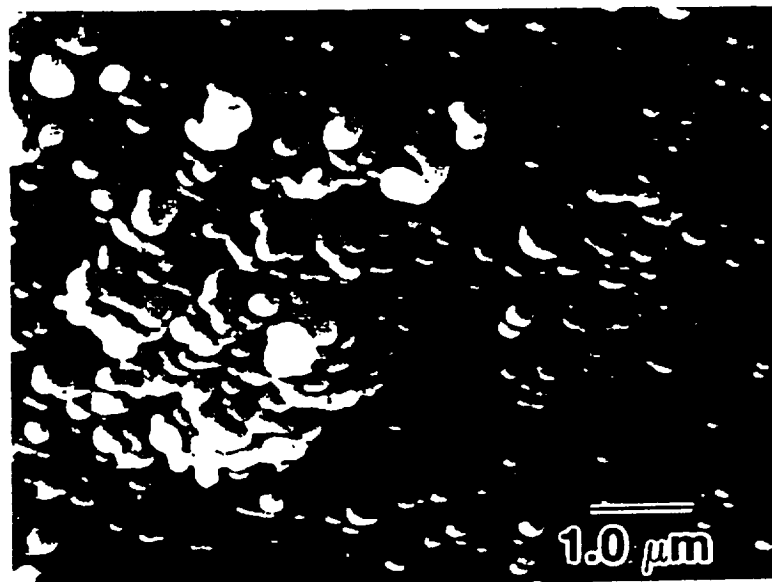

1.0 μm

Figure 8. Surface of sapphire fiber pulled out of matrix during composite tensile test. Lighter phase indicates residual ZrO_2 remaining on fiber surface. Very little pitting or surface damage present on fiber after composite testing and fabrication.

133

Figure 9. Matching primary fiber fracture surfaces from composite tested at 1200°C. Internal flaws identified as fracture origins.

Figure 10. Fracture mirror displaying internal void as critical flaw within the fiber. Composite tested at 1200°C.
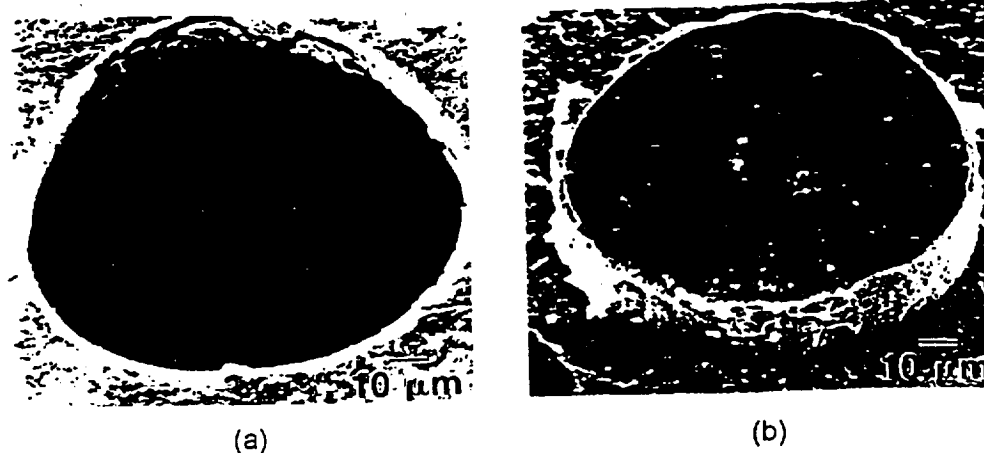
Figure 11. Room temperature fiber push-out test showing both the a) top or pushed in side and b) bottom or pushed out side of the composite.
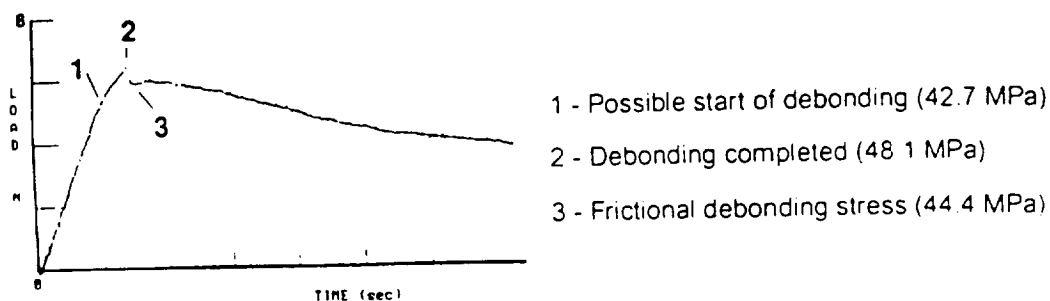

1 - Possible start of debonding (42.7 MPa)

2 - Debonding completed (48.1 MPa)

3 - Frictional debonding stress (44.4 MPa)

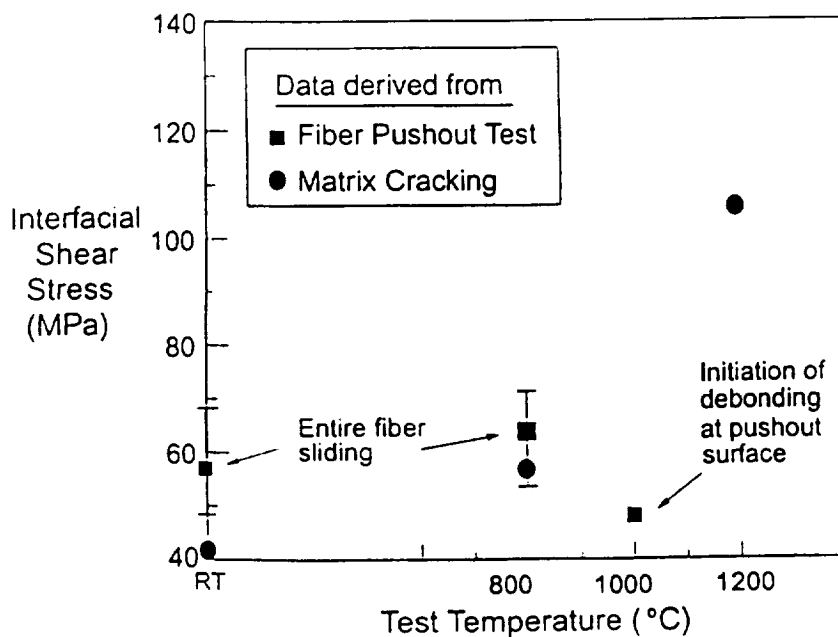Figure 12 Typical load versus time curve from room temperature fiber push-out test

Figure 13 Interfacial shear stress as a function of test temperature. Data derived from either individual fiber push-out tests or matrix crack spacing measured from composite fracture samples tested in tension
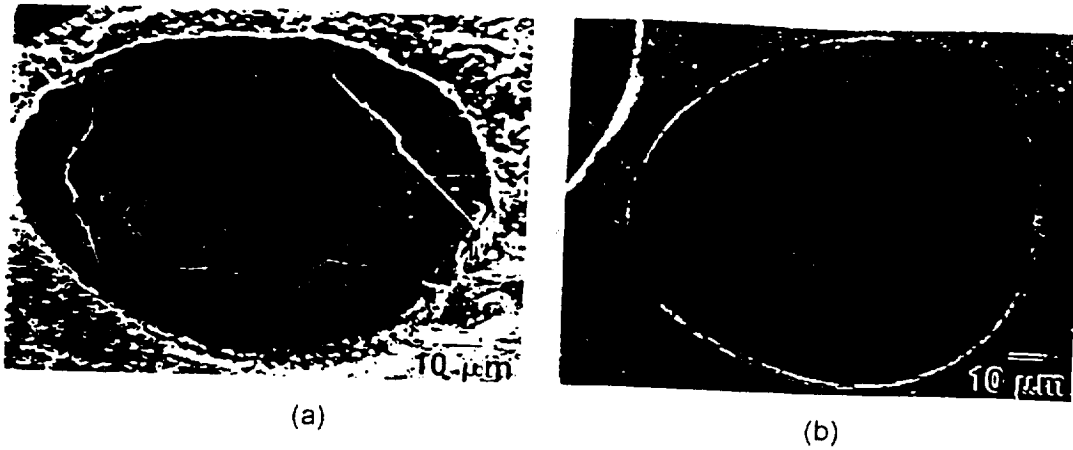
(a)

(b)

Figure 14   Fiber push-out sample tested at 1000°C; a) pushed in side showing plastic deformation caused by indenter. b) pushed in side showing crack propagation through the ZrO₂ coating
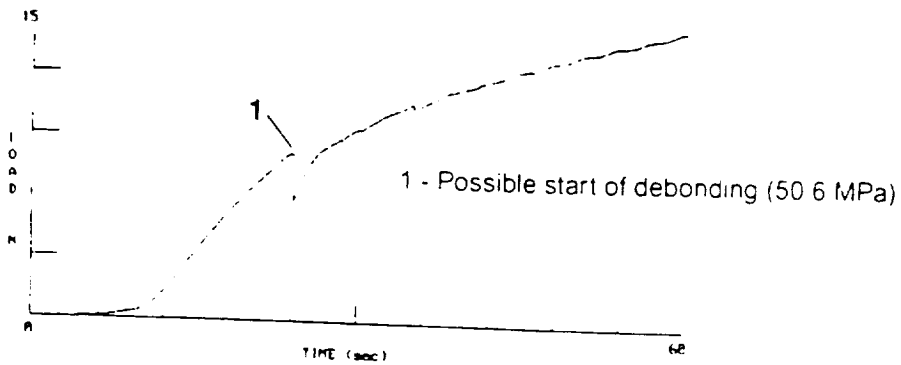

1 - Possible start of debonding (50 6 MPa)

Figure 15   Load versus time curve for 1000"C fiber push-out test   Only initiation of debonding could be identified
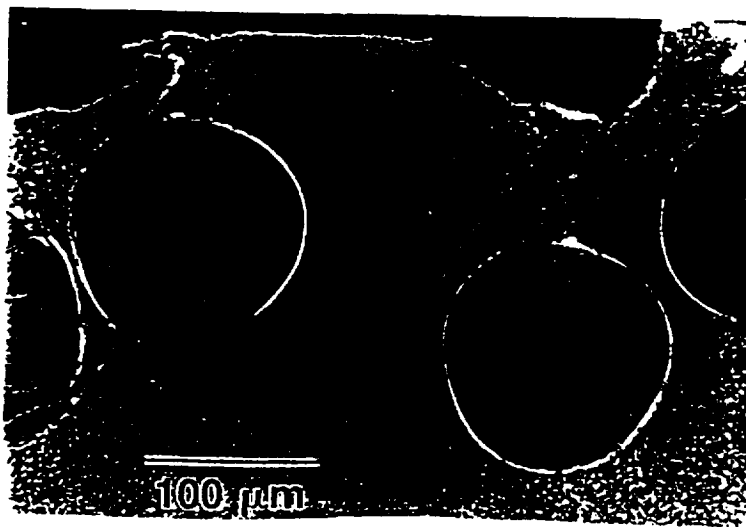

Figure 16   Crack deflection and fiber debonding which occurs during fiber push-out tests at 1000°C

The 21st Annual Conference on Ceramic, Metal and Carbon Composites, Materials, and Structures

Part 1. Ceramics and Ceramic Matrix Composites

And

Part 2. Ceramic Composites for Extreme Environments

January 26-31, 1997
Cocoa Beach, Florida

Proceedings of a Conference:

- Organized and conducted by the Ceramic, Metal, and Carbon Composites Committee (CMC³) with the cooperation of the U.S. Army, U.S. Navy, U.S. Air Force, DARPA, NASA, DOE, and DOC

- Supported by the United States Advanced Ceramics Association (USACA)

- Supported by the National Institute of Ceramic Engineers (NICE)

ROOM TEMPERATURE TENSILE BEHAVIOR AND DAMAGE ACCUMULATION OF HI-NICALON REINFORCED SIC MATRIX COMPOSITES

G.N. Morscher*, Case Western Reserve University, Cleveland, OH

J.Z. Gyekenyesi* , Cleveland State University, Cleveland, OH

ABSTRACT

Composites consisting of woven Hi-Nicalon fibers, BN interphases, and different SiC matrices were studied in tension at room temperature. Composites with SiC matrices processed by CVI and melt infiltration were compared. Monotonic and load/unload/reload tensile hysteresis experiments were performed. A modal acoustic emission (AE) analyzer was used to monitor damage accumulation during the tensile test. Post test polishing of the tensile gage sections was performed to determine the extent of cracking. The occurrence and location of cracking could easily be determined using modal AE. The loss of modulus could also effectively be determined from the change in the velocity of sound across the sample. Finally, the stresses where cracks appear to intersect the load-bearing fibers correspond with high temperature low cycle fatigue run out stresses for these materials.

INTRODUCTION

The high temperature mechanical properties of SiC/SiC composites are limited due to oxidation reactions which occur in the presence of species such as oxygen and water vapor. What enables such reactions to occur at the fiber/interphase/matrix region of a composite is environmental ingress through pores in the matrix and/or through matrix cracks. For SiC/SiC composites where chemical vapor infiltration (CVI) is the matrix processing route, the fiber-matrix interphase region should be sealed off from the environment even though significant matrix porosity exists. Therefore, the environmental reactions are dependent on matrix cracking, although a highly porous matrix will allow the environment access to inner regions of a composite which would not be accessible if the matrix was dense. The composite fabrication method dictates the amount of porosity which exists in the matrix. The loading history of the composite, coupled with the flaw distribution in the matrix, dictate the amount and nature of cracking that exists in the matrix.

An understanding of the damage accumulation in a composite is critical in determining when matrix cracking occurs and the nature of matrix cracking, i.e. local microcracks or through-thickness cracks. Guillaumat and Lamon[1,2] have characterized

---

the damage accumulation in a Nicalon[TM#], C interphase, CVI SiC matrix composite as a function of strain. They found that

1. Microcracks emanate from macropores between different fiber plies and propagate across the plies (ε = 0.025% to 0.12%)
2. Cracks then form and propagate in transverse (90°) bundles and dense matrix regions (ε = ~ 0.12% to 0.2%)
3. Finally, cracks form in the matrix surrounding 0° bundles ($\varepsilon \geq$ 0.2%)

The microcracks formed at large pores in the matrix and in 90° tows are sometimes referred to as tunnel cracks[3-6]. A slight reduction in elastic modulus would be expected from such cracking. When the microcracks intersect and debond the fiber/matrix interphases of the load-bearing fibers, significant elastic modulus reduction and unload/reload hysteresis behavior was observed[6].

This study will compare the stress-strain behavior of woven Hi-Nicalon[TM#], BN interphase, SiC matrix composites with melt infiltrated (MI) and CVI SiC matrices. Modal acoustic emission[7] will be used to monitor the damage accumulation and unload/reload hysteresis loops will be performed to determine the onset of damage in the 0° bundles as well as the interfacial properties of the two composite systems. The findings will then be related to the elevated temperature properties of these two composite systems.

EXPERIMENTAL

Table I: Woven Hi-Nicalon[TM], BN-interphase, SiC Matrix Composites

Composite	Composite Processing Details	Weave	V_f (loading direction)
CVI SiC	CVD BN interphase* CVI SiC matrix*	8 HS	0.15
MI SiC	CVD BN-interphase* 2 μm CVI SiC overcoat* Si melt infiltrated SiC matrix**	5 HS	0.17

- all composites were 0/90 lay ups with 8 plies (17 ends per inch)
* Dupont Lanxide: BN interphase; CVI SiC ** Carborundum: Melt Infiltration SiC
- specific processing details are proprietary

Table I describes the processing approaches, vendors, and woven architectures of the two composites compared in this study. The tensile sample dimensions and mounting arrangement are shown in Figure 1. The samples were cut from 152 mm x 229 mm plates into dogbone tensile specimens where the length was 203 mm, the width at the ends was 12.7 mm and the width at the gage section was ~10.2 mm. The plate thicknesses were nominally 2.35 and 2.2 mm for the CVI SiC and MI SiC composites, respectively. Tensile tests were performed with a screw-driven universal testing machine*. Glass fiber reinforced epoxy tabs (1.5 mm thick) were mounted on both sides of the

---

* Nicalon[TM] and Hi-Nicalon[TM] produced by Nippon Carbon, Japan
* Instron Model 8562, Instron Ltd., Canton, Mass.

sample in the grip regions. The specimens were gripped with rigidly mounted hydraulically actuated wedge grips. A clip on strain gage, with a range of 2.5% strain and 25.4 mm gage length was used to measure strain.

Wide-band (50 kHz to 2.0 MHz)[**], high fidelity sensors (9.2 mm in diameter) were placed just outside the tapered region of the dogbone sample to record acoustic emission events. Vacuum grease was used as a couplant and electrical tape was used to mount the sensors to the sample. Acoustic emission waveforms were recorded using a 2-channel, Fracture Wave Detector[**] (FWD). The FWD consisted of a personal computer (Pentium, 120 MHz) with a 12-bit, 30 MHz analog to digital acquisition board. Each sensor was connected to a preamplifier and filter trigger module which was fed into the computer. The preamplifier was set at 20 dB, the filter signal was amplified 3 dB, and the filter trigger was amplified 21 dB. The load and strain were also recorded with the FWD computer.
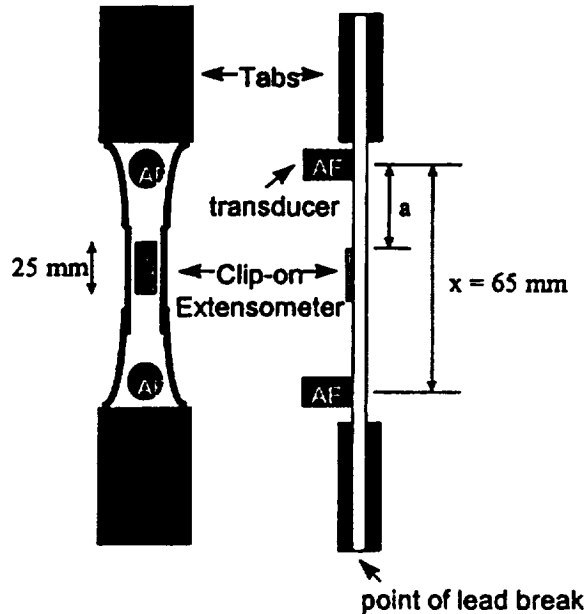
Figure 1: Specimen configuration.

The post-test analysis was performed on Wave Detector™ software provided by the FWD manufacturer.

RESULTS AND DISCUSSION

Typical monotonic tensile stress-strain curves are shown in Figure 2 for the two composites. The stress-strain behavior is very similar to that shown by other researchers for Nicalon/SiC woven composites[8-10]. Both composites failed at similar stresses (~ 380 MPa); however, the MI composites always failed in the grips whereas the CVI composites always failed in the gage section. The "knee" in the stress strain curve occurs at a lower stress for the CVI SiC composites and the strain to failure of the CVI SiC composites is greater than the strain to failure of the MI SiC composite. The mechanical properties of the two composites are listed in Table II.

Figures 3a and b show monotonic and hysteresis stress-strain curves of the two composite systems. The monotonic and hysteresis stress-strain curves are almost identical for both composite systems. The hysteresis stress-strain curves have slightly larger strains for the same stress compared to the monotonic stress-strain curves. For the hysteresis experiments, AE activity occurred in the gage section upon initial unloading and at the end of the subsequent reloading. This indicates a greater amount of damage in the hysteresis specimens[11] and could account for the increased strain incurred for hysteresis tensile tests.

The maximum loop width was determined for each unload/reload hysteresis loop at the stress which was half the maximum stress of the specific loop (Figure 4). The onset of 0° cracking is considered to occur when the hysteresis loop width is greater than zero. This occurs at ~ 110 MPa for CVI SiC composites and ~ 140 MPa for the MI SiC composites. It is also interesting to note that the loop width of the MI SiC composites were greater than that of the CVI SiC composites at higher stresses. It was observed from polished sections of failed composites that CVI SiC composites had almost three times the number of cracks of
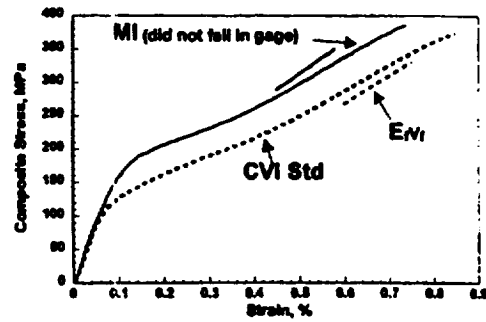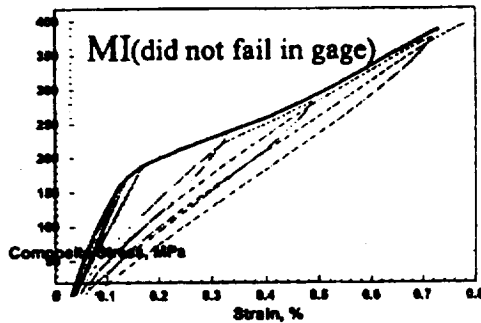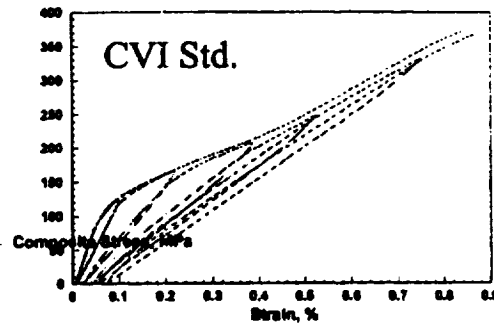

Figure 2: Monotonic stress-strain curves for MI SiC and CVI SiC composites.

(a)

(b)

Figure 3: Monotonic and unload/reload hysteresis tensile stress-strain curves for MI (a) and CVI (b) composites.

MI SiC (Table II).

The modal AE analysis was used to discern the location of events which occurred in the gage section of the composites[11]. This is an important factor to determine because the number of events recorded for the monotonic experiments was ~ 7000 and 9000 for the MI and CVI SiC composites, respectively, whereas only ~ 1500 and 1250 events actually occurred in the gage section for the two composites, respectively. Modal AE analysis, as
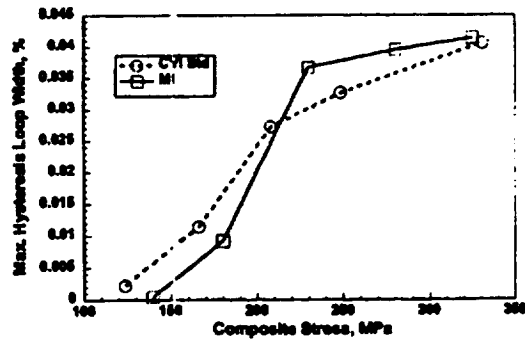

Figure 4: Hysteresis loop width for the two composites versus the peak stress of the hysteresis loop.

4

opposed to traditional AE* , involves the digitization of the real AE waveforms and analysis of the "modes", i.e. extensional (longitudinal) and flexural, of sound travel that make up the individual waveforms.

In order to determine the location of the events, the change in the speed of sound must be known for the stress-strain condition. This was done, as described in ref. 11, for the extensional wave from AE events which occurred outside of the two sensors during the tensile test. If the speed of sound is known as a function of strain, then, the elastic modulus as a function of strain can be determined. The speed of sound of the extensional wave, C_e, is related to elastic modulus, E_o, by:

$C_e = [E_o / \rho (1-\nu^2)]^{1/2}$ (1)

where ρ is the density and ν is Poisson's ratio. The $E_o^{1/2}$ at a given strain can be normalized by $E_o^{1/2}$ at $\varepsilon = 0$ and C_e at a given strain can be normalized by C_e at $\varepsilon = 0$. The normalized $E_o^{1/2}$ and normalized $C_e^{1/2}$ should have the same relationship as shown in Figure 5 for the unload/reload hysteresis tensile tests where E_o was determined from the tangent modulus upon initial unloading of the hysteresis

Figure 5: Normalized $E_o^{1/2}$, $\{E_o(\varepsilon)/E_o(\varepsilon=0)\}^{1/2}$, and normalized C_e, $C_e(\varepsilon)/C_e(\varepsilon=0)$, plotted versus composite strain for the two composites from unload/reload hysteresis tensile experiments.

loop[6]. There is excellent agreement between the reduction in modulus and the reduction in the speed of sound for both composites. In fact the modulus and speed of sound decreases are the same relative to the initial modulus (Table II) and speed of sound of the undamaged material for both composites, respectively. This is not too surprising since both composites appear to have reached or nearly reached matrix crack saturation and both composites failed at similar stress levels which would result in a similar *overall* stress distribution on the fibers over the entire gage length (assuming a constant interfacial shear strength).

The specific gage events were identified from (i) the difference in time of arrival between the two sensors (Figure 1) for a given event and (ii) the change in the speed of sound as the damage in the material increases[11]. Figure 6 shows the AE data for the two composites tested monotonically in tension to failure. The AE data show the same general trend for the two composites. Initially, rapid AE activity is occurring up to the "knee" in the stress strain curve. The rate of AE activity then decreases substantially. For the CVI SiC composite, an increase in the rate of AE activity occurred just prior to
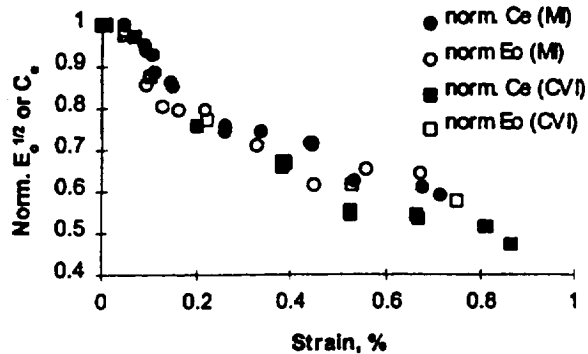
---

* In traditional AE, the real sound wave is fit to a damped sine curve and AE parameters such as counts, amplitude, duration, energy, etc... are tabulated and saved. Resonant frequency transducers are used with traditional AE which cannot detect the wide frequency range of the real waveform that is produced by a fracture event. See references 7 and 11 for greater detail concerning the differences between the two types of AE analysis.

failure; whereas this did not happen for the MI material. The onset of AE activity in the gage section occurred at lower stresses and strains for the CVI composite (Table II). However, the total amount of AE events recorded was greater for the MI composite. It should also be noted that the "loudest" or highest energy events occur predominantly at the lower strains where the rate of AE activity was most rapid[11].

Table II: Results from Tensile Tests

Composite [# tests]	Ultimate Strength (MPa)	Elastic Modulus (GPa)	1st AE Noise Stress (MPa)	1st 0° Cracking Stress (MPa) [LCF stress]#	Avg. Crack Spacing (mm)	Avg. τ (MPa)
CVI Std. [2m, 2h]	370 ± 5	195 ± 5	55	~ 110 [103]	0.34	36 ± 8
MI* [4m, 2h]	>390±5	214 ± 6	74	~ 140 [143]	0.87	11 ± 3

Low Cycle Fatigue (2 hr hold, unload/reload cycle) run out stress (500 hours)
* did not fail in gage section

The tapering off of the AE activity is most likely due to the decrease in matrix cracking or matrix crack saturation (~ 0.35% strain). The inflection in the stress-strain curve is also indicative of matrix crack saturation. The occurrence of AE activity near the ultimate strength for the CVI material is probably due to the initiation of fiber failures in the gage section[11]. This did not happen for the MI material because it did not fail in the gage.
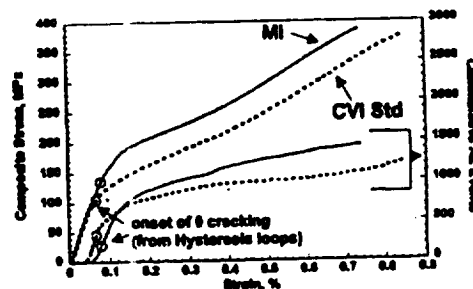

Figure 6: AE activity for monotonic stress strain curves of two composites.

Also noted on Figure 6 is the point on the stress-strain and AE event-strain curves where the onset of 0° cracking was determined (Figure 4). Note that ~ 350 AE events occurred prior to this stress in the CVI material and ~ 200 AE events occurred prior to this stress in the MI material. For the CVI material, the number of AE events occurring prior to the onset of 0° cracks accounts for over 25% of the total number of AE events occurring in the gage section. Evidently, a significant number of microcracks in the matrix and 90° bundles were formed in these materials prior to the extension or formation of cracks which significantly intersect the load-bearing fibers.

The gage sections of the failed composites were cut and polished longitudinally in the gage section to determine the amount and extent of cracking (Figures 7 and 8). For both systems, each crack could essentially be traced completely through the composite from one edge or side of the composite to the other. The cracks appeared to be transverse within a ply, but could deviate up or down between plies. The number of cracks were counted over the length of the gage sections and the average crack spacing was found to be 0.34 mm and 0.87 mm for the CVI and MI composites, respectively. In

other words, nearly three times as many cracks occurred in the gage section for the CVI composites compared to the MI composites.

The most striking difference between the two composites is the porosity of the CVI matrix composite. In the CVI composites, similar to refs. 1 and 2, cracking appeared to emanate primarily from the large, jagged regions (figure 7b) of the pores which existed between 90° tows and in-between plies or on the surface at the intersection of a 0 and 90° tow. For the MI composites, such pores and jagged regions did not exist and it was impossible to discern where the origin of the cracks occurred. Presumably they occurred at surface flaws, large matrix regions, and/or in the 90° bundles.

The interfacial shear stress, τ, was determined from the hysteresis loop width, $\delta\varepsilon_{max}$, and average matrix crack spacing, d_c, for the composites from the relationship[6]:

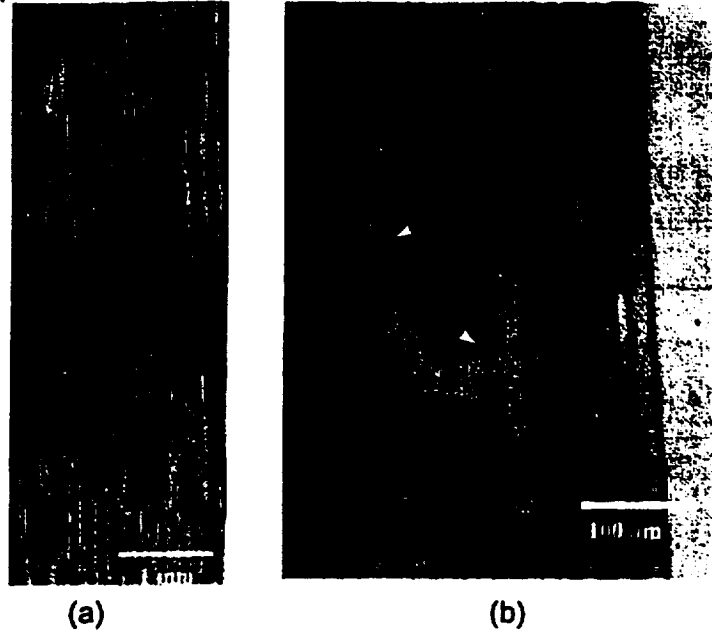(a)   (b)

Figure 7: Lower magnification (a) and higher magnification (b) optical micrographs of polished longitudinal section of CVI composite tested in tension to failure. Arrows indicate cracks.

$$\tau = (\sigma_p^2/2\delta\varepsilon_{max}) \, [b_2(1-a_1v_f)^2(R_f/d_c)/(4v_f^2E_m)] \, (2)$$

where, σ_p is the hysteresis loop peak stress, b_2 and a_1 are coefficients given by Hutchinson and Jensen[12], R_f is the average fiber diameter (13 microns), and E_m is the elastic modulus of the matrix (400 GPa). In order to approximate d_c for each hysteresis loop, the average crack spacing was assumed to be indirectly proportional to the AE activity (similar to Figure 6). For the σ_p of a given hysteresis loop, the final d_c measured after fracture was multiplied by the final number of AE events in the gage and divided by the number of AE events which occurred in the gage up to σ_p. The larger $\delta\varepsilon_{max}$ and d_c for the MI composites resulted in a τ value less than one third that of the CVI composites. This could be due to differing residual stress states from the different matrix processing routes used to fabricate the composites. However, it is most likely that the difference in τ was due to the formation of a carbon layer between the fibers and the BN interphase in the MI composites. The processing temperature for MI SiC is at least that of the melting temperature of Si (~ 1410°C). The Hi-Nicalon™ fibers undergo some decomposition above about 1400°C which results in the formation of a carbonaceous layer at the surface of the fiber[13]. Transmission electron microscopy studies on similar composites have shown that a thin carbon layer does exist between the fiber and the BN for Hi-

7

Nicalon™/BN/MI SiC composites and has not been observed for Hi-Nicalon™/BN/CVI SiC composites[14].

The nature of damage accumulation is expected to influence the elevated temperature life properties of CMC's. Some data exists[15-16] for low-cycle fatigue, LCF, tests performed on these same types of composites at 815°C in air. The LCF cycle consisted of a loading step to the peak stress, a 2 hour hold at the peak stress followed by an unloading step down to a minimum stress value. The run-out condition for these experiments was set at 250 cycles (500 hours at the peak stress). It was found that the run-out stresses for the CVI and MI composites were 103 MPa and 143 MPa respectively. These are nearly identical with the onset of 0° cracking as determined from the hysteresis tensile tests (Table II). Evidently, for this composite life
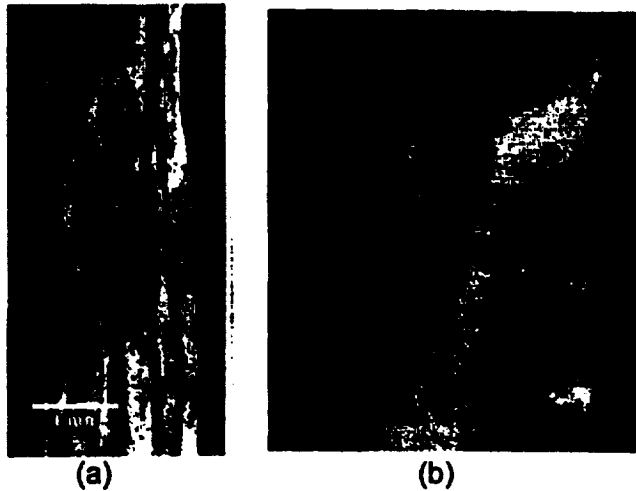

(a)   (b)

Figure 8: Lower magnification (a) and higher magnification (b) optical micrographs of polished longitudinal section of MI composite tested in tension to failure. Arrows indicate cracks.

criteria, the stress where the onset of cracking occurs was not life limiting. Instead, it was the stress where crack growth or crack formation resulted in the intersection of the load-bearing fibers. The LCF peak stress was about twice the stress at which cracking was first detected in the gage section of these composites. This of course assumes that the onset of cracking at 815°C is the same as at room temperature. Lipetzky et al[10] have shown that for a Nicalon-CVI SiC composite the modulus, proportional limit and damage regime slope of the tensile stress-strain curve up to 1200°C is essentially unchanged. Since these properties do not change it is reasonable to assume that the onset of cracking is essentially the same over this temperature range.

CONCLUSION

The mechanical properties and damage accumulation of Hi-Nicalon, BN interphase woven composites with CVI SIC and MI SIC matrices were determined and compared. The ultimate and elastic properties of the two composites were similar; however, the onset of cracking occurred at lower stresses and strains for the CVI composite system. This was due to the large, jagged pores which exist in the CVI SiC matrix and were the site of initial cracking for these composites. MI SiC matrix composites did not have such pores. Modal acoustic emission was found to be a useful technique to monitor the onset and continuum of damage which occurred *in the gage section* of the tensile specimens tested. The decrease in the speed of sound as increasing damage occurred with increasing stress could be used to determine the elastic modulus with increasing damage accumulation.

Fewer cracks occurred in the gage section for MI composites due to the lower interfacial shear strength of these composites. It was presumed that the lower interfacial strength of the MI composites was due to the formation of a carbon layer at the fiber matrix interphase due to the decomposition of the fibers during processing.

Finally, the stresses for both composite systems where cracks intersected the load-bearing bundles (0° cracking) could be correlated to the life-limiting stresses from

elevated temperature low cycle fatigue tests performed in air at 815°C; even though cracking had occurred in the composites at stresses which were half the stress for 0° cracking.

ACKNOWLEDGEMENT

REFERENCES

1. L. Guillaumat and J. Lamon, "Multi-fissuration de Composites SiC/SiC," in Revue des Composites et des Materiaux Avances, vol. 3, pp. 159-171 (1993)
2. L. Guillaumat and J. Lamon, "Probabilistic-Statistical Simulation of the Non-Linear Mechanical Behavior of a Woven SiC/SiC Composite," Comp. Sci. Tech., 56, 803-808 (1996)
3. D.S. Beyerle, S.M. Spearing, and A.G. Evans, "Damage Mechanisms and the Mechanical Properties of a Laminated 0/90 Ceramic/Matrix Composite," J. Am. Ceram. Soc., 75, 3321-30 (1992)
4. S. Ho and Z. Suo, "Tunneling Cracks in Constrained Layers," J. Appl. Mech., 60, 890-94 (1993)
5. Z.C. Xia, R.R. Carr, and J.W. Hutchinson, "Transverse Cracking in Fiber Reinforced Brittle Matrix, Cross-Ply Laminates," Acta Metall. Mater., 41 [8] 2365-76 (1993).
6. J.M. Domergue, F.E. Heredia, and A.G. Evans, "Hysteresis Loops and the Inelastic Deformation of 0/90 Ceramic Matrix Composites," J. Am. Ceram. Soc., 79 [1] 161-70 (1996)
7. M. R. Gorman, "New Technology for Wave Based Acoustic Emission and Acousto-Ultrasonics," AMD-Vol. 188, Wave Propagation and Emerging Technologies, ASME, pp. 47-59 (1994)
8. M. Leparoux, L. Vandenbulcke, S. Goujard, C. Robin-Brosse, and J.M. Domergue, "Mechanical Behavior of 2D-SiC/BN/SiC Processed by ICVI," Proc. ICCM-10, Vol. IV, 633-640 (1995).
9. C. Droillard and J. Lamon, "Fracture Toughness of 2-D Woven SiC/SiC CVI-Composites with Multilayered Interphases," J. Am. Ceram. Soc., 79[4] 849-58 (1996)
10. P. Lipetzky, G.J. Dvorak, N.S. Stoloff, "Tensile Properties of a SiCf/SiC Composite," Mater. Sci. Eng. A216 pp. 11-19 (1996).
11. G.N. Morscher, "Modal Acoustic Emission of Damage Accumulation in a Woven SiC/SiC Composite," submitted to Comp. Sci. Tech.
12. J.W. Hutchinson and H. Jensen, "Models of Fiber Debonding and Pull-Out in Brittle Composites with Friction," Mech. Mater., 9, 139-63 (1990)
13. G. Chollon, R. Pailler, R. Naislain, F. Laanani, M. Monthioux, and P. Olry, "Thermal Stability of a PCS-derived SiC Fibre with a Low Oxygen Content (Hi-Nicalon)," J. Mater. Sci., 32, 327-47 (1997)
14. J. Brennan, unpublished research.
15. D. Brewer, NASA Lewis Research Center, unpublished research.
16. G.N. Morscher, "Embrittlement of Hi-Nicalon™, BN, CVI and MI SiC Matrix Composites in Air at Elevated Temperatures, " to be presented at the 1998 Annual American Ceramic Society Meeting.